Wintertime sub-arctic new particle formation from Kola Peninsula sulphur emissions

Mikko Sipilä[1], Nina Sarnela[1], Kimmo Neitola[1], Totti Laitinen[1], Deniz Kemppainen[1], Lisa Beck[1], Ella-Maria Duplissy[1], Salla Kuittinen[1,2], Tuuli Lehmusjärvi[1], Janne Lampilahti[1], Veli-Matti Kerminen[1], Katrianne Lehtipalo[1,2], Pasi P. Aalto[1], Petri Keronen[1], Erkki Siivola[1], Pekka A. Rantala[1], Douglas R. Worsnop[1,3], Markku Kulmala[1], Tuija Jokinen[1], Tuukka Petäjä[1]

[1]Institute for Atmospheric and Earth System Research, PO. Box 64, 00014, University of Helsinki, Finland
[2]Finnish Meteorological Institute, 00560, Helsinki, Finland
[3]Aerodyne Research Inc. 01821 Billerica, MA, USA

Correspondence to: Mikko Sipilä (mikko.sipila@helsinki.fi)

Abstract. Metallurgical industry in Kola Peninsula, North-West Russia, form, after Norilsk, Siberia, the second largest source of air pollution in the Arctic and sub-Arctic domain. Sulphur dioxide (SO_2) emissions from the ore smelters are transported to wide areas, including Finnish Lapland. We performed investigations on concentrations of SO_2 and aerosol precursor vapours, aerosol and ion cluster size distributions together with chemical composition measurements of freshly formed clusters at the SMEAR I station in Finnish Lapland relatively close (~300 km) to the Kola Peninsula industrial sites during the winter 2019-2020. We show that highly concentrated SO_2 from smelter emissions is converted to sulphuric acid (H_2SO_4) with sufficient concentrations to drive new particle formation hundreds of kilometres downwind from the emission sources, even at very low solar radiation intensities. Observed new particle formation is primarily initiated by H_2SO_4-ammonia (negative-) ion induced nucleation. Particle growth to cloud condensation nuclei (CCN) sizes was concluded to result from sulphuric acid condensation. However, air mass advection had a large role in modifying aerosol size distributions, and other growth mechanisms and condensation of other compounds cannot be fully excluded. Our results demonstrate the dominance of SO_2 emissions in controlling winter-time aerosol and CCN concentrations in the subarctic region with a heavily polluting industry.

1 Introduction

Sulphur dioxide (SO_2) is one of the main air pollutants, influencing the acidification of soils and freshwaters, defoliation and reduced vitality of forests, atmospheric aerosol formation, cloud properties, and adverse health effects by air pollutants. Anthropogenic SO_2 originates primarily from the combustion of fossil fuels at power plants, other manufacturing complexes and ships, as well as from the smelting of sulphur-containing mineral ores. Because of the severe environmental and health effects by SO_2, efforts have been made in order to suppress its emissions to the atmosphere. While the global SO_2 emissions have not shown any rapid decay, emissions in e.g. OECD (Organisation for Economic Co-operation and Development) countries have decreased significantly within last 3 decades (Solarin and Tiwari, 2020).

1

The metallurgical industry with large-scale smelter complexes in the Kola Peninsula, North-West Russia, form the second largest source of air pollution in the Arctic and sub-Arctic region. Smelters emit large quantities of SO_2, metals and particulate matter to the atmosphere. These pollutants, especially SO_2, have large impacts on both atmosphere and biosphere in the surrounding area, including the eastern parts of Finnish and Norwegian Lapland. In the close proximity of industrial plants, these pollutants have literally destroyed ecosystems, creating "industrial deserts" (Paatero et al., 2008). Though emissions have significantly decreased from ca. 600 kilotons yr^{-1} in early 1990's (Tuovinen et al., 1993; Ekimov et al., 2001), partly because of the collapse of Soviet Union and related socio-economical changes in Russia, they are still high. Today, Kola peninsula SO_2 emissions are around 200 kilotons yr^{-1} (Barentz Observer, 2019), far higher than the SO_2 emissions of the whole Finland (37 kilotons yr^{-1} in 2017). Though vast, Kola emissions are still far behind the emissions of the World's number one SO_2 polluter, Norilsk (Krasnoyarsk Krai, Northern Siberia), with enormous 1.5 megatons yr^{-1} emission rates (Barentz Observer, 2019). Together with the few other smaller-scale industrial complexes, these smelters are almost the sole local sources of air pollution in the very sparsely populated (sub-)Arctic Eurasia, and therefore understanding their role in atmospheric chemistry and physics is of great importance.

In the atmosphere, SO_2 can be photochemically oxidized to sulphuric acid (H_2SO_4) in the gas phase. While most of the atmospheric sulfate is formed from SO_2 in a liquid phase in cloud droplets, which may evaporate leading to sulfate aerosol production or precipitate as acid rain, with very high concentrations of SO_2 in the Kola Peninsula area also high production rates of gas-phase H_2SO_4 are expected. The H_2SO_4 vapour can, in turn, contribute to atmospheric new particle formation (NPF) via nucleation and subsequent particle growth even up to sizes of cloud condensation nuclei (CCN) by further condensation of H_2SO_4 and potentially some other vapours (e.g. Weber et al., 1995; Kirkby et al., 2011; Jokinen et al., 2018). Atmospheric NPF is an important process because, according to model simulations, it accounts for more than a half of atmospheric CCN formation globally (Merikanto et al., 2009; Gordon et al., 2017). At high latitudes, the contribution of NPF has been estimated to be even larger, reaching >90% of the cloud level CCN in the high Arctic and approximately 70-80% in our study area, the sub-Arctic zone of Northern Finland and North-Western Russia (Gordon et al., 2017).

Vehkamäki et al. (2004) were the first to report observations of NPF (> 8 nm diameter particles) at the Värriö SMEAR I field station in eastern Lapland, Finland, relatively close to the Kola Peninsula smelter complexes. Their results on the contribution of SO_2 pollution were not completely definitive, so that during the four years of measurements 15 out of the 147 observed NPF events were concluded to be explained by SO_2 pollution plumes. Kyrö et al. (2014) recorded particle number size distributions down to 3 nm in diameter and showed that NPF is connected to high concentrations of SO_2. They observed NPF even during winter in almost dark conditions, indicating that during episodes of very high concentrations of SO_2, a sufficient fraction of it is converted to H_2SO_4 in the gas phase even in very low solar radiation levels to initiate NPF. However, to date, no reports on

115 quantification of sulphuric acid concentrations by direct measurements, or detailed mechanisms and chemical compounds involved in NPF, in this area exist.

While observation of atmospheric NPF has been reported in hundreds of publications since the times of John Aitken (Aitken, 1900), the details, i.e. the dynamics and contributing compounds, of NPF have been experimentally resolved only in a limited
120 number of atmospheric environments. Pioneering studies include the observations by Weber et al. (1995) on the connection between sulphuric acid and atmospheric nucleation, and the first report on ion-induced nucleation and simultaneous detection of sulphuric acid anion clusters using a mass spectrometer by Eisele et al. (2006). Among the field work, several laboratory investigations by the same research groups probed the properties of sulphuric acid – water and sulphuric acid – ammonia – water clusters and their potential role in new particle formation (Ball et al., 1999; Hanson and Eisele, 2002).
125

Later advances in understanding the *molecular* steps of nucleation and growth in the atmosphere include the discovery that iodic acid (HIO$_3$) is primarily responsible for nucleation and growth in coastal areas and in the vicinity of the Arctic sea ice (Sipilä et al., 2016; Baccarini et al., 2020). Jokinen et al. (2018) demonstrated that in coastal Antarctica, H$_2$SO$_4$ originating from the oxidation of dimethyl sulphide (DMS, emitted by pelagic phytoplankton) and ammonia (NH$_3$, from penguin colonies)
130 nucleate via a negative ion-induced mechanism, with sulfuric acid condensation accounting for most of the subsequent particle growth. Further observations on nucleation mechanisms indicate the key role of highly oxidized organic molecules HOM (Ehn et al., 2014) in NPF during the spring-summer time in a boreal forest environment (e.g. Kulmala et al., 2013; Rose et al., 2018) and in the mid-latitude continental free troposphere (Bianchi et al., 2016) in parallel with sulfuric acid – ammonia nucleation (Bianchi et al., 2016; Schobesberger et al., 2015; Yan et al., 2018). Dimethyl amine has been found to contribute to initial
135 nucleation in polluted urban air (Yao et al., 2018). In addition to these, yet rare molecular-level atmospheric observations, several laboratory studies have investigated the details of these nucleation mechanisms (e.g. Kirkby et al., 2011; Almeida et al., 2013; Kürten et al., 2014; Kirkby et al., 2016). Recent laboratory studies that probed nucleation of nitric acid and ammonia suggest the mechanism may contribute to new particle formation and growth especially in the upper troposphere (Wang et al., 2020).
140

Mass spectrometers (Junninen et al., 2010; Jokinen et al., 2012) and air ion spectrometers (Mirme and Mirme, 2013), have largely facilitated the recent progress in the field of atmospheric NPF. By utilizing them in conjunction with aerosol and meteorological observations, this work aims to shed light on the molecular steps of NPF resulting from (sub-)Arctic air pollution during wintertime. Investigations were carried out at the SMEAR I research station in Värriö strict nature reserve in
145 Finnish Lapland close to the industrial plants (most of them located approximately 300 km east from the station) of Kola Peninsula, north-west Russia, during the winter 2019 – 2020.

2 Methods

2.1 Site and time of the study

160 Measurements were carried out at the Värriö SMEAR I research station (Hari et al., 1994) located in Värriö strict nature reserve, Finnish Lapland, in the vicinity (5 km) of Russian border (Fig. 1) (67°45′19″N 29°36′37″E). The station stands on a top of a hill (390 m a.s.l.), being surrounded by untouched pine and spruce forests, bogs, fells, small lakes and rivers. Several large smelter complexes are located ~300 km away from to the station on the Russian side of the border, while on the Finnish side no smelters or other large-scale energy intensive (polluting) industrial plants are located within a distance of several hundreds

165 of km – the closest, relatively small coal burning plant is located 550 km away. The SMEAR I station was set up in 1991 for monitoring air pollution, especially sulphur dioxide (SO_2) originating from the Kola Peninsula smelters. In this work we present 4.5 months data from winter time, 1st November 2019 until 16th March 2020.

2.2 Instrumentation

Aerosol number size distribution between 3 and 750 nm was recorded by a twin differential mobility particle sizer (DMPS)

170 (Aalto et al., 1999), comprising Hauke-type differential mobility analyzers (lenghts 110 and 280 mm) and TSI-3776 and TSI-3772 condensation particle counters (TSI Inc., Shoreview, MN, USA) as detectors. The other DMPS malfunctioned during 9th – 10th and 14th – 27th January, resulting in the loss of data on 3 – 10 nm particles.

Number size distribution of charged particles and molecular clusters between 0.8 and 40 nm was recorded by a Neutral Cluster

175 and Air Ion Spectrometer (NAIS, Airel Ltd., Estonia, Mirme & Mirme, 2013).

Aerosol precursor vapour concentrations, H_2SO_4, methane sulphonic acid (MSA), HIO_3 and HOM were measured by a nitrate ion – Chemical Ionization -Atmospheric Pressure interface – Time-Of-Flight mass spectrometer (CI-APi-TOF, Jokinen et al., 2012), equipped from 26th January onwards with a switcher inlet, with which the instrument can switch between chemical

180 ionization (CI) operation mode and natural ion detection mode. This instrument was calibrated in the CI-mode for sulphuric acid, as described by Kürten et al. (2012). A same calibration coefficient was used for reported MSA and HIO_3. However, the instrument was not fully operational at all the times during the measurement campaign and significant fraction of data (including all collected prior 25th December and a long period in January) was disregarded.

185 SO_2 was recorded with a TEI 43 i-TLE pulsed fluorescence analyzer, O_3 by a TEI 49 i photometric analyzer, and NO_x by a TEI 42C TL chemiluminescence analyzer with photolytic NO_2-to-NO converter, all manufactured by Thermo Fischer Scientific (Franklin, MA, USA). The wind speed and direction as well as the air temperature were measured with a Vaisala WTX sensor 16 m above ground level.

4

2.3 Nucleation rate calculation

Negative (-) and positive (+) ion-induced nucleation rates of 1.5 nm particles, $J^{-/+}_{1.5}$, were calculated assuming a steady-state between formation and loss of particles in the size range of 1.5 and 2.5 nm:

210

$$J^{-/+}_{1.5} = \frac{dN^{-/+}_{1.5-2.5}}{dt} + \frac{GR_2}{\varDelta d_p} N^{-/+}_{1.5-2.5} + CoagS\, N^{-/+}_{1.5-2.5} + k_{rec} N^{+/-}_{<1.5} N^{-/+}_{1.5-2.5} \qquad (1)$$

where $N^{-/+}_{1.5-2.5}$ is the total concentration of negative or positive ions in the size range between 1.5 and 2.5 nm, filtered using Matlab's Savitzky-Golay 2nd order filtering method to remove the instrument noise, k_{rec} is the recombination coefficient
215 between negative and positive small ions which was here approximated by a size-independent constant of $1.6 \cdot 10^{-6}$ cm^3 s^{-1} (Tammet, 1995), $N^{+/-}_{<1.5}$ is the concentration of positive or negative sub-1.5 nm cluster ions. GR_2 is the 2 nm particle growth rate, $\varDelta d_p$ is the width of the size interval for which the concentration is defined ($\varDelta d_p$ = 2.5 nm – 1.5 nm = 1 nm), and $CoagS$ is the coagulation sink of 2 nm particles to the pre-existing background aerosol population. CoagS was calculated from the following equation:

220

$$CoagS = \sum_{i=1}^{n} K_{2nm,i} N_i \qquad (2)$$

where N_i is the concentration of particles in the channel i of DMPS and $K_{2nm,i}$ is the coagulation coefficients between a 2-nm particle and a particle in the size bin i calculated based on Seinfeld and Pandis (1998).

225

An accurate determination of the particle growth rate for 2 nm particles from the size distribution is challenging, and therefore GR_2 was approximated by assuming irreversible sulphuric acid condensation as the sole mechanism of growth similar to Jokinen et al. (2018) and Beck et al. (2021) according to (Stolzenburg et al., 2020):

230
$$GR_2 = 1.45 \cdot \left(2.68 \cdot \left(\frac{d_p}{nm} \right)^{-1.27} + 0.81 \right) \cdot [H_2SO_4] \cdot 10^{-7} \text{molec.}^{-1} \text{cm}^3 \qquad (3)$$

where the pre-factor 1.45 accounts for dipole - charge interaction in charged particle growth (Stolzenburg et al., 2020). The justification for this approach will be discussed later. More standard method for GR determination is to approximate GR_2 by the average growth rate of the formed particle population, including mainly particles grown far above the 2 nm size, during a
235 few hours starting from the beginning of the event as demonstrated in Figure 2A. This method leads to average GR of 4.5 nm h^{-1}. However, this approach neglects the effect of air mass advection which, as will be discussed later, may largely determine the time development of the size distribution and thus also the apparent growth.

5

Rather than the average GR of the whole particle population, the 50-% appearance time method (Lehtipalo et al. 2014) could be used to estimate the growth rate of nucleating clusters in the size range of 1.3 – 2.7 nm (Figure 2B). Here, the cluster appearance time in each size channel represent the time when cluster concentration reaches 50% of its maximum concentration during the event. Growth rate can be assessed from the cluster diameter vs. appearance time curve (black line) resulting in ~0.35 nm h^{-1} between 10:10-11:30 and in ca. 1.8 nm h^{-1} growth during 11:30-11:50 and the average growth rate of ~0.9 nm h^{-1} during the period from 10:10-11:50. Drawback of this analysis is that the GR cannot be obtained for the period where concentration has passed the 50%-threshold or the period of decaying concentration. Furthermore, temporal GR cannot be properly obtained due to fluctuations in the data. Nevertheless, above mentioned values of 0.35 – 1.8 nm h^{-1} can be compared to those obtained from Eq. 3, which yields maximum GR during the example day (29th January 2020) of 0.51 nm h^{-1} around noon. Comparison to 1.8 nm h^{-1} obtained from the 50%-appearance time method slightly before noon leads to a factor of ~3.5 difference in GR_2 on that day, which, in turn, is reflected in 22% difference in the calculated nucleation rate (Eq. 1). Effect of different determination of GR are visualized in Figure S1. To conclude, ion-induced nucleation rate calculation is not very sensitive to GR_2 because ion-ion recombination term (Eq. 1) dominates the loss in our conditions.

2.4 Sulphuric acid proxy calculation

Because of significant gaps in the measured data, [H$_2$SO$_4$] was also calculated using a proxy developed by Dada et al. (2020). This proxy takes into account the oxidation of SO$_2$ to H$_2$SO$_4$ both by OH (estimated from the global radiation intensity) and stabilized Criegee Intermediates (estimated from monoterpene and ozone concentrations; Sipilä et al., 2014), as well as losses of H$_2$SO$_4$ by dimerization (negligible in observed concentrations) and condensation onto pre-existing aerosol particles (the primary loss term). Unfortunately, there are no VOC measurements available at SMEAR I, but because the data were collected during winter well outside of the growth period, we assumed the monoterpene concentration to be zero. Global radiation measurements showed unexplained fluctuations (maybe caused by low solar zenith angles or freezing of the sensor) during the measurement period, and therefore we used UVB radiation and the relation between UVB and global radiation determined by Dada et al. (2020). During the times when CI-APi-TOF was operational, the agreement between the measured and calculated concentrations was good (Figure S2) with mean concentrations agreeing within 8%. Obtained correlation coefficient was R = 0.790 and coefficient of determination R^2 = 0.624.

2.5 Trajectory analyses

Trajectories were calculated by using the Hybrid Single-Particle Lagrangian Integrated Trajectory model HYSPLIT (Stein et al., 2015) with GFS 0.25 degree meteorology as an input. We calculated 24-hour backward trajectories arriving at 50 and 250 meters above ground level for the period 28.1.2020 00UTC to 30.1.2020 00 UTC, arriving every 6 hours. The trajectory calculations included mixing layer depth along the trajectory.

6

3 Results and Discussion

3.1 New particle formation during the measurement period.

Figures 3a & 4a depict the aerosol number size distribution between 3 and 700 nm, as recorded by the DMPS. Several new particle formation events were observed during the measurement period. Clear NPF events with concentration of 4 -10 nm particles, N_{4-10nm}, (Figures 3b & 4b) exceeding 50 cm^{-3} are marked with grey shadings. Since the DMPS data on sub 10-nm particles were missing from 9th -10th and 14th – 27th January, N_{4-10nm} could not be derived for those time periods. Still, at least on 18th and 19th January we can see NPF that eventually produces particles larger than 10 nm in diameter. The observed NPF events coincided mostly (ca. 50% of the cases) with clearly easterly (~90°) winds (Figures 3c & 4c) and elevated H_2SO_4 concentrations (Figures 3d & 4d) calculated based on Dada et al. (2020). H_2SO_4 concentrations depend, besides condensation sink and UVB radiation, on the SO_2 concentration which is connected to both wind direction and air mass origin. Clear examples of such, SO_2 pollution driven NPF events are, for example, those occurring during three consecutive days on 10th - 12th November, 2019, two days on 28th – 29th January, 2020, and on 13th March, 2020. The data from 28th – 29th January are discussed in detail below, whereas the data from the other two exemplary periods are presented in the Supplement (Figures S3 – S11).

Not all the NPF events occurred during the easterly winds. The events observed close to mid-winter, from early December until early January, occurred with westerly winds or during the transition of wind direction from west to east, in relatively low concentrations of SO_2 and in the virtual absence of day light and H_2SO_4. These low-H_2SO_4 mid-winter events were observed to start from sizes larger than a few nm, which means that nucleation did not take place in-situ in the surroundings of the SMEAR I station. Those particles had thus formed elsewhere and were transported to the measurement site by horizontal advection, or vertically down from above the mixed layer. Compared with particles of a few nm in diameter, gas-phase H_2SO_4 is lost much more rapidly onto pre-existing particles after its production ceases, so the lack of H_2SO_4 is not excluding its primary role in NPF though not supporting such role either. Some of the mid-winter NPF events coincided with elevated SO_2 concentrations suggesting that sulphuric acid may have be formed in the measured air mass earlier, while some, especially the relatively strong NPF event on December 3rd presented in the Supplement (Figures S9-S11), occurred in a virtual absence of SO_2 suggesting that sulphuric acid had not been formed to a significant extent in that air mass. Currently, we thus cannot explain the mechanism of NPF on that day. However, the NO_2 concentration was slightly (Figure S9) elevated in the measured air mass, which might have been connected with the elevated source of particles. Nevertheless, most of the NPF events seemed to be connected with the presence of H_2SO_4.

7

3.2 Case study 28th – 29th January 2020

To resolve the details of new particle formation and growth, we focus on 3 time periods with clearly occurring nucleation and particle growth. Here we show results from analysis of a 2-day period from 28th – 29th January 2020. To demonstrate that the discussed 2-day period is not only a unique observation, we represent data from time periods of 10th -12th November, 2019 (Figures S3-S5) and 13th March, 2020 (Figures S6-S8) in the Supplement. The data from the event on 3rd December, 2019, which differs from the overall picture, are also depicted in the Supplement (Figures S9-S11).

3.2.1 Meteorological situation and trace gas concentrations

Throughout the period of 28th – 29th January, the wind was blowing from the East (~50 - 150°) (Figure 5a). The ambient temperature ranged from -16°C to -28°C (Figure 5b). The sky was clear but, because of the low solar zenith angle (maximum 4.4° at noon 29th Jan.), the UVB radiation intensity needed for a photochemical H_2SO_4 formation reached only 35 mW m^{-2} (summertime UVB radiation intensity maxima at Värriö are >2000 mW m^{-2}). The HYSPLIT back trajectory calculations showed that air masses arriving between January 28th at 6:00 and January 30th at 00:00 passed the industrial areas of the Montchegorsk region (Figure 6).

At around 3:00 on 28th January coinciding with the change in the air mass origin to the Montchegorsk-Kandalaksha region (Figure 6) (a few hours after the change of wind direction from west to east in the evening of 27th January), air pollutant levels started to increase steeply (Figure 5d). During the course of the day, both SO_2 and NO_2 concentrations increased several orders of magnitude, with [SO_2] peaking at 27 ppb and [NO_2] at 7 ppb. Ozone (O_3) concentration declined from about 40 ppb to a 30 ppb range. To put the high level of SO_2 concentrations into some perspective, the highest concentration recorded at the Helsinki Metropolitan area was 8.4 ppb (24 µg m^{-3}, 1-hour average) in 2019 and the yearly average concentration was about 0.2 ppb (~0.5 µg m^{-3}) (Helsinki Region Environmental Services Authority, 2020). The yearly average SO_2 concentration at the SMEAR I station in 2019 was 1.1 ppb.

3.2.2 Aerosol precursors

Despite the low UVB radiation, required for O_3 photolysis that initiates H_2SO_4 production via OH radical formation, H_2SO_4 concentration increased from close to the lowest detection limit values of ~10^5 molecules cm^{-3} up to $8 \cdot 10^5$ molecules cm^{-3} during 28th and up to $1.5 \cdot 10^6$ molecules cm^{-3} on 29th (Figure 7e). Because the OH production rate must have been low, high SO_2 concentration is a perquisite for the H_2SO_4 production during cold and dark winter months. Though stabilized Criegee Intermediates (sCI) formed in alkene ozonolysis can oxidize SO_2 to produce H_2SO_4 during summertime (Mauldin et al., 2012; Sipilä et al., 2014), alkene (terpene) emissions from the vegetation and thus the sCI production rate are negligible during the winter season. Proxy calculations agree well with the measured sulphuric acid concentration on 29th but show clearly higher

8

values on 28th January. The cause of the disagreement on 28th January is probably the stable and shallow boundary layer. The temperature gradient close to the surface was almost +0.2 °C m⁻¹ at noon on 28th (Figure 5b). Solar radiation from close the horizon is not penetrating efficiently inside the canopy, so the UVB measured above canopy and used in the proxy calculation does not reflect the situation at the ground level. Sulphuric acid produced above the canopy, on the other hand, does not mix downwards due to the strong temperature inversion and calm winds. On 29th January, the temperature gradient was absent or slightly negative, allowing the surface air to mix with the air above canopy.

Besides H_2SO_4, also minute signals of iodic acid (HIO_3) were observed during the day (Figure 7e). The exact production mechanism of HIO_3 remains globally unknown despite the emerging evidence on its critical role in new particle formation especially in the Arctic regions (Sipilä et al., 2016; Baccarini et al., 2020). Methane sulphonic acid (MSA), that has been observed in larger aerosol particles (Beck et al., 2021) and that could potentially also contribute to NPF, hardly exceeds the detection threshold. This was expected since MSA originates from dimethyl sulphide (DMS) photo-oxidation. DMS ends up into the air mainly from the metabolism of pelagic phytoplankton during summer months, not during the dark winter. No other condensable vapours, such as HOM which dominate the new particle growth in the summer-time boreal forest environment (Ehn et al., 2014), were observed during this case study period or during other periods depicted in Supplement.

3.2.3 New particle formation

Ion size distribution

Figures 7a and 7b show the NPF events on 28th and 29th January, as observed by the NAIS operated in the ion mode. Omnipresent small, < 1.5 nm ions are continuously produced by the galactic cosmic radiation, terrestrial gamma radiation and gas phase radon decay. Approximately at 11:00 on 28th January, coinciding with the increase of the H_2SO_4 concentration, small negative cluster ions started to grow, which is seen as small increases in the ~1.5–2 nm negative ion concentration. During their growth beyond ~2 nm in diameter, those clusters were neutralized by collisions with positively charged ions so that they disappeared from the spectrum. They still obviously continued their growth, as charged particles reappeared in the spectrum after reaching some 5 nm in diameter when diffusion charging becomes effective enough; an equilibrium charging state for 2 nm particles is 0.8% while 5 nm particles are charged with an efficiency of 2.3% and out of 20 nm particles 11% are negatively charged (Wiedensohler et al., 2012). Opposite to negative ions, positive cluster ions did not grow in size. Larger, > 5nm positive particles (charged by diffusion charging during the course of their growth) grew similarly to negative particles. On 29th January, with clearly higher H_2SO_4 concentrations, the appearance of >1.5 nm negative clusters was more pronounced, suggesting higher rates of nucleation and critical role H_2SO_4 in the initial steps of NPF. Positive cluster ions were again only bystanders and did not contribute to nucleation. This observation suggests negative ion-induced nucleation as the primary pathway to new particle formation similar to $H_2SO_4 – NH_3 (– H_2O)$ ion-induced nucleation observed by Jokinen et al. (2018)

9

in Antarctica and Kirkby et al. (2011) in CERN CLOUD chamber experiments. However, due to lack of information on neutral ~1.5–3 nm cluster concentrations, this observation alone does not exclude parallel neutral nucleation mechanisms.

Nucleation rates

Even though weak growth of the small negative ions around noon on 28th January is visually observable in Figure 7a, the concentration of clusters in the 1.5–2.5 nm size range ($N^-_{1.5-2.5}$) is hardly distinguishable from the noise (Figure 7c). Nucleation rate, calculated using filtered concentration data, only slightly exceeded the baseline (caused by presence of minute, almost omnipresent signal from ion clusters extending above 1.5 nm but which is not connected to sulphuric acid nucleation), being approximately 0.005 cm^{-3} s^{-1} with a high relative uncertainty (Figure 7d). On 29th, with a 2.3-fold sulphuric acid concentration, the concentration of 1.5–2.5 nm negative clusters was well above the instrument noise reaching 20 cm^{-3} s^{-1} around the noon. The nucleation rate peaked at 0.067 cm^{-3} s^{-1}. The ambient temperatures during nucleation (~ noon) were close identical, around –22°C, in both days and therefore they can be directly compared. An approximately 10-fold difference in the nucleation rate between the two days accompanied by a factor of 2.3 difference in the sulphuric acid concentration is in line with the results from the CLOUD-chamber experiment on sulphuric acid – ammonia – water nucleation (Kirkby et al., 2011). The so-called "slope" that approximately (not exactly in real atmospheric situations) equals to the number of sulphuric acid molecules in the critical cluster (Vehkamäki et al., 2012) is given as:

$$Slope = \frac{d\log J^-_{1.5}}{d\log[H_2SO_4]}$$

and yields a value of 2.9 for the numbers discussed above. Though this value is subject to a significant uncertainty, it would agree with observations of Kirkby et al. (2011) and parameterizations by Dunne et al. (2016) which yield a "slope" of approximately 3 under similar conditions as visualized in Figure 8. In the same figure, data from all days with clearly observable ion-induced nucleation are depicted. There, hourly average nucleation rates $J_{1.5^-}$, that exceed a threshold value of $J_{1.5^-} = 0.01$ cm^{-3} s^{-1}, are plotted against the concurrent calculated sulphuric acid concentration and air temperature. Calculated nucleation rates, J_{GCR}, represent the total nucleation rates (ion-induced plus neutral) in different temperature and ammonia concentrations under influence of galactic cosmic radiation (GCR) producing ions with the fixed rated of 1.8 ion pairs cm^{-3} s^{-1}. Negative ion-induced nucleation, however, should be the dominant mechanism under these conditions (Kirkby et al., 2011) and results can be therefore compared. Our data is reasonably close to range predicted by parameterization considering that this simple calculation does not include airmass transportation, vertical mixing, terrestrial radiation sources, or any other real-world phenomena. Also, sources and concentration of ammonia in our study area are unknown.

10

Cluster time series

635

To confirm the role of sulphuric acid and to solve the contribution of ammonia in the nucleation process, we measured the negative ion cluster composition and signal intensity with the APi-TOF in the ion mode without chemical ionization. The time series of the most abundant clusters show the appearance of HSO_4^- - ion in the morning of 28th Jan together with increasing $[H_2SO_4]$ accompanied with a decay of NO_3^- - ion which typically dominates the anion spectrum at low $[H_2SO_4]$ and low $[HIO_3]$

640 globally (Figure 7f). Since H_2SO_4 is a stronger acid than HNO_3, proton transfers from H_2SO_4 to NO_3^- explain the observed behaviour when $[H_2SO_4]$ started to rise. When $[H_2SO_4]$ still increased during the course of the day, $(NH_3)_m(H_2SO_4)_nHSO_4^-$ - clusters started to form. The cluster signals peaked at around the noon coinciding with the highest $[H_2SO_4]$ and $N_{1.5-2.5}^-$ after which they started to decay. On 29th January, the same behaviour was observed, but with somewhat stronger cluster signals due to the higher $[H_2SO_4]$.

645

Cluster composition

To get more insight into the chemical composition of clusters, the ion-cluster mass spectrum was integrated over 4 hours (2 hours effective data collection due to switching between CI and ion-inlet). The resulting spectrum is presented in Figure 9 by

650 means of a mass defect plot, where the mass-to-charge ratio (m/z, unit Th) corresponds – with only singly charged ion clusters present in the air – to the mass of the cluster (m, unit Da, equal to unified atomic mass unit, u). Mass defect is the mass difference (in Th or Da) between the exact mass of the cluster and the integer mass defined as the sum of nucleons in the atomic nuclei of the cluster; for example, the exact mass of a HSO_4^- -ion that has 97 nucleons is 96.960103 Da and the mass defect is thus 0.039896 Da. The area of a dot is proportional to the logarithm of the observed signal intensity. In the mass

655 defect plot each addition of a molecule or atom is represented by a vector. Addition of e.g. H_2SO_4, with a negative mass defect, leads to an increasing mass and a decreasing total mass defect, while an addition of a positive mass defect NH_3 molecule leads to an increasing total mass defect. Successive additions of certain molecules to an ion results in a straight line in the mass defect plot, so that different cluster formation pathways are readily distinguishable from the plot.

660 In Figure 9, the largest signals are associated with omnipresent nitrate ion and its cluster with nitric acid (NO_3^- and $HNO_3 \cdot NO_3^-$). The rest of the small (<180 Da) ions are mainly different sulphur species, with bisulphate ion partly clustered with nitric acid (HSO_4^- and $HNO_3 \cdot HSO_4^-$) being most abundant. Other small sulphur ions present in the spectrum are SO_4^-, SO_5^-, $HNO_3 \cdot SO_3^-$ and $HNO_3 \cdot SO_4^-$. Deprotonated iodic acid (IO_3^-) and its nitric acid cluster, ($HNO_3 \cdot IO_3^-$) are also abundant. Despite multiple different types of these core ions, their initial growth is caused solely by the attachment of sulphuric acid molecules. We

665 observed clusters with 1-4 H_2SO_4 molecules attached to the SO_4^- - ion one H_2SO_4 molecule attached to the to SO_5^- and SO_3^- - ions, and 1-3 H_2SO_4 molecules attached to the IO_3^- -ion. For simplicity, we assume that the negative charge remains in the core

Deleted: 5
Deleted: ing
Deleted: s
Deleted: s
Deleted: C
Deleted:
Deleted: is

Deleted: 6
Deleted:

Deleted: A
Deleted: the
Deleted: ,
Deleted: ,
Deleted: to
Deleted: the

Commented [KV16]: tää täytyy lisätä tähän, muuten lukija putoaa kärryiltä puhutaanko vielä kuvasta 6 vai onko tämä jotain yleistä tietoa.

Deleted: 6
Deleted: L
Deleted: R
Deleted: of them
Deleted: solely

ion. This is not necessarily true, but H_2SO_4 may lose a proton e.g. to IO_3^- resulting in the composition of $HIO_3 \cdot (H_2SO_4)_{n-1} \cdot HSO_4^-$ instead of $^-(H_2SO_4)_n \cdot IO_3^-$. Furthermore, water, if present in the clusters, efficiently evaporates in the vacuum of the mass spectrometer and therefore information on the role of water in the cluster formation is lost.

690

None of the above discussed clusters seem to adopt ammonia efficiently enough for their signals to exceed the detection threshold of the APi-TOF (mass dependent, $\sim10^{-3}$ to few 10^{-3} ions/second for 2 hour integration for m/z > 400 Th). Only clusters made solely of sulphuric acid with a bisulphate ion (HSO_4^-) as a core seem to efficiently attach ammonia, resulting in the formation of $(NH_3)_m \cdot (H_2SO_4)_n \cdot HSO_4^-$ -clusters (n>=3). This sequential addition of NH_3 and H_2SO_4 has been shown to be

695 an effective (ion-induced) cluster formation and growth mechanism in coastal Antarctica (Jokinen et al., 2018) as well as a secondary pathway in the free troposphere (Bianchi et al., 2016) and in the spring/summer time southern Finland boreal forest (Yan et al., 2018).

Our results on negative cluster composition can be compared to the results from the CLOUD experiment at -25°C for varying
700 NH_3/H_2SO_4 - ratio (Schobesberger et al., 2015). Based on that data, with the NH_3/H_2SO_4 - ratio exceeding approximately 100, both cluster composition and nucleation rate saturate (Kirkby et al., 2011) and become unaffected by further increases of the NH_3 concentration. In those conditions, a cluster comprising 3 molecules of sulphuric acid on a bisulphate ion, $(NH_3)_n \cdot (H_2SO_4)_3 \cdot HSO_4^-$, contains on average approximately n~1 molecules of ammonia, whereas a cluster composed of 4 molecules of sulphuric acid and a bisulphate ion, $(NH_3)_n \cdot (H_2SO_4)_4 \cdot HSO_4^-$, carries on average approximately n~1.5 NH_3 molecules
705 (Schobesberger et al., 2015). In our case (Figure 9), corresponding average ammonia numbers were n~0.4 and n~0.8 for $(NH_3)_n \cdot (H_2SO_4)_3 \cdot HSO_4^-$ and $(NH_3)_n \cdot (H_2SO_4)_4 \cdot HSO_4^-$, respectively, which would suggest that the NH_3/H_2SO_4 – ratio in our case was well below 100, and likely below 10 (Schobesberger et al., 2015). If true, that would indicate an ammonia concentration of the order of $\sim10^7$ molecules cm^{-3}, or ~1 pptv. However, cluster fragmentation inside the mass spectrometer can be totally different between our experiment and Schobesberger et al. (2015) study and therefore any conclusions on ammonia
710 concentration should not be drawn. Nevertheless, if NH_3/H_2SO_4 – ratio would be low, that would mean that the system is not saturated with respect to NH_3 and that the nucleation rate should therefore be sensitive to both H_2SO_4 *and* NH_3 similar to Jokinen et al. (2018). This together with unknown effects of cluster fragmentation, highlight the importance of understanding NH_3 sources, transportation and atmospheric mixing ratios down to ppt levels for a proper description of new particle formation also in the subarctic region. Unfortunately, NH_3 concentrations in the range of 1 pptv are not (reliably) detectable with any
715 present-day measurement technology.

The present analysis shows that sulphuric acid – ammonia ion-induced nucleation can trigger new particle formation in the winter time sub-arctic / boreal environment with a high level of anthropogenic SO_2 pollution but a low UV-radiation intensity. Data on neutral 1.5-3 nm particles are not available, so that neutral nucleation rates could not be derived. However, based on

12

740 all the evidence obtained from field (mainly Jokinen et al., 2018) and especially from CLOUD experiments (Kirkby et al., 2011; Schobesberger et al., 2015), in the absence of significant amounts of compounds other than H_2SO_4 and NH_3, and with the nucleation rates being below the ion pair production rate (typically 2-4 ion pairs cm^{-3} s^{-1} in the Earth's surface layer), ion induced nucleation seems to dominate over the neutral one. In our case, HOM were below the detection limit, and amines, if important, would appear also in the anion spectrum in H_2SO_4 clusters. HIO_3 and MSA were present, but significant neutral

745 homogeneous nucleation of HIO_3 would require ~100-fold concentration of it compared to what was measured here (Sipilä et al., 2016).

The observation of clusters containing IO_3^- or HIO_3 together with H_2SO_4 is, however, highly interesting. HIO_3 has been shown to nucleate homogeneously, and also mixed clusters containing both HIO_3 and H_2SO_4 have been reported from the Alps (Frege

750 et al., 2017), the Atlantic coast (Sipilä et al., 2016) and the Arctic (Beck et al., 2021). If the SO_2 rich pollution plumes from the smelters are advected to iodine source areas (arctic ocean and especially sea ice zone as well as macroalgae rich coasts) or vice versa, this mixed mechanism may become important.

3.2.4 Particle growth and relevance for CCN-concentrations

Based on the above analysis, particle nucleation is clearly driven by sulphuric acid and ammonia, with the nucleation rate

755 being most probably sensitive to concentrations of both of these vapours. But how do the freshly nucleated clusters grow? Assuming irreversible condensation, even the peak sulphuric acid concentration of $1.5 \cdot 10^6$ molecules cm^{-3} can explain only a small fraction of the observed growth rate. Consistent with an earlier report on wintertime particle growth rates at Värriö (Kyrö et al., 2014), the apparent average growth rate on 29th January was approximately 4.5 nm h^{-1} (Figure 2), which, based on Stoltzenburg et al. (2020), would require a steady concentration of ca. $2.6 \cdot 10^7$ molecules cm^{-3} throughout the growth process

760 which continues long after the sunset and the decay of $[H_2SO_4]$. Obviously, there are two possible explanations for this disagreement: either sulphuric acid is not responsible for most of the growth, or the air is not homogenous and the apparent growth is caused by the air mass advection.

Besides sulphuric acid, the only condensable vapours detected are MSA and HIO_3 (and NH_3). However, their concentrations

765 are clearly lower than that of sulphuric acid, and therefore condensation of those in a homogeneous air mass cannot explain the apparent growth either. It could be speculated that compounds not recorded by CI-APi-TOF, such as SO_2 or some less oxidized volatile or semi-volatile organic compounds, (S)VOC, condense or react in particle phase forming low volatile compounds thereby contributing to growth (Stolzenburg et al., 2018), but a complete absence of highly oxidized compounds does not support, though not fully exclude either, the presence of less oxidized compounds at a high abundancy. The NO_2

770 concentration was moderate, up to 7 ppb, and therefore also nitric acid concentrations were likely insufficient to have a measurable effect on the growth (Wang et al., 2020). However, the temperature was low during the studied time period and

13

therefore HNO_3 or some other semi-volatile compound could have contributed to the growth, provided that such compounds were present. Ammonia was detected in small ion clusters but its contribution to the particle volume concentration, assuming that the measured cluster NH_3/H_2SO_4 ratio reflects the composition of larger particles, was marginal. Assuming the particle composition to be ammonium bisulphate, i.e. NH_3/H_2SO_4 -ratio of unity, ammonia would contribute 17% to the particle volume and 5% to particle diameter growth rate.

The most plausible explanation for the observed growth is that the particle growth is driven by H_2SO_4 condensation but its concentration is not uniform over the source area. In that case, particles would nucleate and grow to their final sizes during the few hours of sunlight. Particles formed and grown in the close environment of emissions sources with high SO_2 and thus H_2SO_4 concentrations grow to larger sizes than particles formed near the measurement site. Air mass advection would then transport particles through the dark hours, leading to a steadily increasing nucleation (and later Aitken) mode diameters at SMEAR I observed as apparent steady growth even through the night. Modelling efforts and measurement of chemical composition or hygroscopicity of growing modes would be required for an unambiguous explanation of the particle growth.

New particle formation in the sub-Arctic winter would be irrelevant if formed particles would not grow to sizes (above few tens of nm) where they can act as CCN. We did not measure CCN concentrations at different supersaturations, but the air masses arrived from the Murmansk–Kandalaksha region from about 03:00 onwards on 28th January (Figure 6) contained elevated concentrations of Aitken and accumulation mode particles mainly in the size range of ~20 – 500 nm (Figure 10). New particle formation clearly increased the concentration of >3 nm particles, and also the concentration of particles larger than 50 nm showed an increase, especially on 29th January. The concentration of particles larger than 100nm was relatively constant and apparently unaffected by NPF during the times when these NPF events could be observed. Air mass advection and particle loss processes, however, naturally have an impact on measured concentrations and are largely responsible for the development of particle populations.

Figure 11 presents the average particle number size distribution during the about a one-week period of eastern winds (28th Jan – 3rd Feb 2020) when the two clear NPF events presented above occurred. Concentrations of particles in all the size classes were remarkably higher, even an order of magnitude for 10-200 nm particles, than the average concentrations during the preceding and succeeding time period with westerly winds. Concentrations during that one-week period were also clearly higher than the average concentrations between 1st November and 29th February, suggesting that new particle formation may be a significant source of particles in the eastern air masses. However, primary emissions from the smelters and the surrounding cities would naturally show up in the size distribution plot as well. A more thorough analysis is needed to separate the roles of secondary NPF and primary emissions in the aerosol and CCN budgets. March, with almost constant NPF was excluded from this analysis since the lighting conditions in March differ significantly from those of early November – end of February.

14

For an accurate assessment of contribution of secondary aerosol formation to CCN concentrations at SMEAR I or regionally, meteorological situation, including boundary layer dynamics, wet deposition of particles, etc. should be considered. However, our observations on clearly elevated CCN-sized aerosol concentrations in eastern airmasses (Figs. 10 & 11) point towards a clear contribution of Kola Peninsula SO_2 emissions to winter-time CCN concentrations in the region.

4 Conclusions

Winter-time new particle formation and growth was investigated at the SMEAR I station, in Värriö strict nature reserve, Finnish Eastern Lapland. Sulphur dioxide concentration in the airmasses arriving from Kola peninsula were often very high, occasionally over 30 ppb. In these high concentrations enough sulphuric acid formed even in very low solar radiation intensity to initiate new particle formation and growth.

New particle formation was observed mostly, but not solely, with easterly winds and in airmasses arriving from the direction of Kola peninsula smelters. Newly formed (4-10 nm, concentration > 50 cm^{-3}) particles were observed in altogether 34 days between 1st November 2019 and 15th March 2020 out of which ca. 60% were associated with eastern winds or with the period of wind direction change from ~west to east. Nucleation was observed in-situ at SMEAR I at H_2SO_4 concentration exceeding ca. $1 \cdot 10^6$ molec. cm^{-3}. These cases were identified based on the appearance of ~1.5-2 nm ion clusters. Other NPF events were observed as appearances of a few nm particles which gradually grew in size over time. Nucleation at SMEAR I was shown to proceed via a negative ion-induced sulphuric acid – ammonia (– water) channel which, based on prior understanding from laboratory experiments, can be hypothesized to dominate the NPF process at our site. Closer to SO_2 emission sources where H_2SO_4 concentrations are likely remarkably higher, nucleation can proceed also via neutral channel and could, theoretically, involve compounds other than H_2SO_4, NH_3 and water.

Larger particles with a diameter of at least a few nm observed at SMEAR I, were probably formed out of the immediate vicinity of the site and they had grown during the air mass advection. Secondary aerosol formation from Kola emissions together with primary particle emissions impact the aerosol size distribution, clearly increasing the concentrations of particles in all the size classes, and therefore unavoidably also CCN concentrations. For better understanding of the contribution of Kola SO_2 emissions to local and regional CCN concentrations and upscaling our results to cover the whole (sub)-arctic Eurasia with vastly polluting industrial cities such as Norilsk, require more measurements. Those measurements should be complemented by CCN or cloud residual measurements – ideally in more than only one location (SMEAR I) around the Kola peninsula. Regional chemical transport and aerosol dynamic modeling would be necessary for thorough assessment.

15

Data availability. Mass spectrometer and air ion spectrometer data related to this article are available from Zenodo as well as upon request to the corresponding author. Rest of the data are available for download from https://smear.avaa.csc.fi/preview.

Supplement. The supplement related to this article is available online at:

Author contributions. MS designed the experiment, MS, NS, KN, TL, DK, SK, LB, TL, JL, PPA, PK, ES, PAR, and TJ prepared the instruments, performed calibrations, collected the data and processed the data, MS and NS analyzed the data, EMD calculated the back trajectories. MS wrote the manuscript. All authors contributed to the interpretation of data and commented in manuscript.

Competing interests. The authors declare that they have no conflict of interest.

References

Aalto, P., Hämeri, K., Becker, E., Weber, R., Salm, J., Mäkelä, J. M., Hoell, C., O'Dowd, C. D., Karlsson, H., Hansson, H.-C., Väkevä, M., Koponen, I. K., Buzorius, G., and Kulmala, M.: Physical characterization of aerosol particles during nucleation events, Tellus, 53B, 344–358, 2001.

Aitken, J. (1900). On some Nuclei of Cloudy Condensation. Transactions of the Royal Society of Edinburgh, 39(1), 15-25. doi:10.1017/S0080456800034025.

Almeida, J., Schobesberger, S., Kürten, A., Ortega, I. K., Kupiainen-Määttä, O., Praplan, A. P., Adamov, A., Amorim, A.,Bianchi, F., Breitenlechner, M., David, A., Dommen, J., Don-ahue, N. M., Downard, A., Dunne, E., Duplissy, J., Ehrhart, S.,Flagan, R. C., Franchin, A., Guida, R., Hakala, J., Hansel, A., Heinritzi, M., Henschel, H., Jokinen, T., Junninen, H., Kajos, M.,Kangasluoma, J., Keskinen, H., Kupc, A., Kurtén, T., Kvashin,A. N., Laaksonen, A., Lehtipalo, K.,

16

Leiminger, M., Leppä,J., Loukonen, V., Makhmutov, V., Mathot, S., McGrath, M. J.,Nieminen, T., Olenius, T., Onnela, A., Petäjä, T., Riccobono, F.,Riipinen, I., Rissanen, M., Rondo, L., Ruuskanen, T., Santos, F.D., Sarnela, N., Schallhart, S., Schnitzhofer, R., Seinfeld, J. H.,Simon, M., Sipilä, M., Stozhkov, Y., Stratmann, F., Tomé, A.,Tröstl, J., Tsagkogeorgas, G., Vaattovaara, P., Viisanen, Y., Vir-tanen, A., Vrtala, A., Wagner, P. E., Weingartner, E., Wex, H.,Williamson, C., Wimmer, D., Ye, P., Yli-Juuti, T., Carslaw, K.S., Kulmala, M., Curtius, J., Baltensperger, U., Worsnop, D. R.,Vehkamäki, H., and Kirkby, J: Molecular understanding of sulphuric acid - amine particle nucleation in the atmosphere, Nature, 502, 359–363, https://doi.org/10.1038/nature12663, 2013.

Ball, S. M., Hanson, D. R., Eisele, F. L., and McMurry, P. H.: Laboratory studies of particle nucleation: Initial results for H_2SO_4, H_2O, and NH_3 vapors, J. Geophys. Res., 104, 23709–23718, doi:10.1029/1999JD900411, 1999.

Baccarini, A., Karlsson, L., Dommen, J., Duplessis, P., Vüllers, J., Brooks, I. M., Saiz-Lopez, A., Salter, M., Tjernström, M., Baltensperger, U., Zieger, P., and Schmale J.: Frequent new particle formation over the high Arctic pack ice by enhanced iodine emissions. Nat Commun. 11, 4924-. https://doi.org/10.1038/s41467-020-18551-0, 2020.

Bianchi, F., Trostl, J., Junninen, H., Frege, C., Henne, S., Hoyle,C. R., Molteni, U., Herrmann, E., Adamov, A., Bukowiecki, N.,Chen, X., Duplissy, J., Gysel, M., Hutterli, M., Kangasluoma, J.,Kontkanen, J., Kürten, A., Manninen, H. E., Münch, S., Peräkylä,O., Petäjä, T., Rondo, L., Williamson, C., Weingartner, E., Cur-tius, J., Worsnop, D. R., Kulmala, M., Dommen, J., and Baltensperger, U.: New particle formation in the free troposphere: A question of chemistry and timing, Science, 352, 1109–1112,https://doi.org/10.1126/science.aad5456, 2016.

Dada, L., Ylivinkka, I., Baalbaki, R., Li, C., Guo, Y., Yan, C., Yao, L., Sarnela, N., Jokinen, T., Daellenbach, K. R., Yin, R., Deng, C., Chu, B., Nieminen, T., Wang, Y., Lin, Z., Thakur, R. C., Kontkanen, J., Stolzenburg, D., Sipilä, M., Hussein, T., Paasonen, P., Bianchi, F., Salma, I., Weidinger, T., Pikridas, M., Sciare, J., Jiang, J., Liu, Y., Petäjä, T., Kerminen, V.-M., and Kulmala, M.: Sources and sinks driving sulfuric acid concentrations in contrasting environments: implications on proxy calculations, Atmos. Chem. Phys., 20, 11747–11766, https://doi.org/10.5194/acp-20-11747-2020, 2020

Ehn, M., Thornton, J., Kleist, E., Sipilä, M., Junninen, H.,Pullinen, I., Springer, M., Rubach, F., Tillmann, R., Lee, B.,Lopez-Hilfiker, F., Andres, S., Acir, I.-H., Rissanen, M., Joki-nen, T., Schobesberger, S., Kangasluoma, J., Kontkanen, J., Nieminen, T., Kurtén, T., Nielsen, L. B., Jørgensen, S., Kjaer-gaard, H. G., Canagaratna, M., Maso, M. D., Berndt, T., Petäjä, T., Wahner, A., Kerminen, V.-M., Kulmala, M., Worsnop,D. R., Wildt, J., and Mentel, T. F.: A large source of low-volatility secondary organic aerosol, Nature, 506, 476–479, https://doi.org/10.1038/nature13032, 2014.

Eisele, F. L., Lovejoy, E. R., Kosciuch, E., Moore, K. F., Mauldin III, R. L., Smith, J. N., McMurry, P. H., and Iida, K.: Negative atmospheric ions and their potential role in ion-induced nucleation, J. Geophys. Res., 111, D04305, doi:10.1029/2005JD006568, 2006.

995

Ekimov S.V., Samodova I.V., Petrov I.M., Troitsky V.V., and Burstein M.A.: Russian smelter emissions, Mining Journal, London, November 23, p. 393, 2001.

Gordon, H., Kirkby, J., Baltensperger, U., et al.: Causes and importance of new particle formation in the present-day and preindustrial atmospheres, J. Geophys. Res.-Atmos., 122, 8739–8760, https://doi.org/10.1002/2017JD026844, 2017.

000

Hanson, D. R. and Eisele, F. L.: Measurement of prenucleation molecular clusters in the NH_3, H_2SO_4, H_2O system, J. Geophys. Res., 107, 4158, doi:10.1029/2001JD001100, 2002.

005

Hari, P., Kulmala, M., Pohja, T., Lahti, T., Siivola, E., Palva, L., Aalto, P., Hämeri, K., Vesala, T., Luoma, S., and Pulliainen, E.: Air pollution in eastern Lapland: challenge for an environmental research station, Silva Fenn., 28, 29–39, 1994.

Helsinki Region Environmental Services Authority, 2020.

010

Jokinen, T., Sipilä, M., Junninen, H., Ehn, M., Lönn, G., Hakala,J., Petäjä, T., Mauldin III, R. L., Kulmala, M., and Worsnop, D. R.: Atmospheric sulphuric acid and neutral cluster measurements using CI-APi-TOF, Atmos. Chem. Phys., 12, 4117–4125, doi:10.5194/acp-12-4117-2012, 2012.

015

Jokinen, T., Sipilä, M., Kontkanen, J., Vakkari, V., Tisler, P., Du-plissy, E.-M., Junninen, H., Kangasluoma, J., Manninen, H. E., Petäjä, T., Kulmala, M., Worsnop, D. R., Kirkby, J., Virkkula, A.,and Kerminen, V.-M.: Ion-induced sulphuric acid–ammonia nu-cleation drives particle formation in coastal Antarctica, Sci. Adv.,4, eaat9744, https://doi.org/10.1126/sciadv.aat9744, 2018.

020

Junninen, H., Ehn, M., Petäjä, T., Luosujärvi, L., Kotiaho, T., Kos-tiainen, R., Rohner, U., Gonin, M., Fuhrer, K., Kulmala, M., and Worsnop, D. R.: A high-resolution mass spectrometer to measure atmospheric ion composition, Atmos. Meas. Tech., 3, 1039–1053, doi:10.5194/amt-3-1039-2010, 2010.

https://julkaisu.hsy.fi/ilmanlaatu-paakaupunkiseudulla-vuonna-2019-1.html#cLhM3ZB0tQ

025

Kirkby, J., Curtius, J., Almeida, J., Dunne, E., Duplissy, J., Ehrhart, S., Franchin, A., Gagne, S.,Ickes, L., Kürten, A., Kupc,A., Metzger, A., Riccobono, F., Rondo, L., Schobesberger,S., Tsagkogeorgas, G., Wimmer, D., Amorim, A., Bianchi,F., Breitenlechner, M., David, A., Dommen, J.,Downard,A., Ehn, M., Flagan, R. C., Haider, S., Hansel, A., Hauser, D., Jud, W., Junninen, H., Kreissl, F., Kvashin, A., Laaksonen, A., Lehtipalo, K., Lima, J., Lovejoy, E. R.,
030   Makhmutov, V., Mathot, S., Mikkila, J., Minginette, P., Mogo, S., Nieminen, T., Onnela, A., Pereira, P., Petäjä, T.,Schnitzhofer,R.,Seinfeld, J. H., Sipilä, M., Stozhkov, Y., Stratmann,F., Tome, A., Vanhanen, J., Viisanen, Y.,Vrtala, A., Wagner, P. E., Walther, H., Weingartner, E., Wex, H., Winkler, P. M., Carslaw, K. S., Worsnop, D. R., Baltensperger, U., and Kulmala, M.: Role of sulphuric acid, ammonia and galactic cosmic rays in atmospheric aerosol nucleation., Nature, 476,429–433, doi:10.1038/nature10343, 2011.

035

Kirkby, J., Duplissy, J., Sengupta, K., Frege, C., Gordon, H.,Williamson,C., Heinritzi, M., Simon, M., Yan, C., Almeida, J.,Tröstl, J., Nieminen, T., Ortega, I. K., Wagner, R., Adamov, A.,Amorim, A., Bernhammer, A.-K., Bianchi, F., Breitenlechner, M., Brilke, S., Chen, X., Craven, J., Dias, A., Ehrhart, S., Flagan,R. C., Franchin, A., Fuchs, C., Guida, R., Hakala, J., Hoyle, C.R., Jokinen, T., Junninen, H., Kangasluoma, J., Kim, J., Krapf,M., Kürten, A., Laaksonen, A.,
040   Lehtipalo, K., Makhmutov, V., Mathot, S., Molteni, U., Onnela, A., Peräkylä, O., Piel, F., Petäjä, T., Praplan, A. P., Pringle, K., Rap, A., Richards, N. A. D., Riipinen, I., Rissanen, M. P., Rondo, L., Sarnela, N., Schobesberger, S., Scott, C. E., Seinfeld, J. H., Sipilä, M., Steiner, G., Stozhkov,Y., Stratmann, F., Tomé, A., Virtanen, A., Vogel, A. L., Wagner, A., Wagner, P. E., Weingartner, E., Wimmer, D., Winkler, P. M., Ye, P., Zhang, X., Hansel, A., Dommen, J., Donahue, N.M., Worsnop, D. R., Baltensperger, U., Kulmala, M., Carslaw, K.S., and Curtius, J.: Ion-induced nucleation of pure biogenic
045   particles, Nature, 533, 521–526, https://doi.org/10.1038/nature17953, 2016.

Kulmala, M., Kontkanen, J., Junninen, H., Lehtipalo, K., Manni-nen, H. E., Nieminen, T., Petäjä, T., Sipilä, M., Schobesberger,S., Rantala, P., Franchin, A., Jokinen, T., Järvinen, E., Äijälä, M.,Kangasluoma, J., Hakala, J., Aalto, P. P., Paasonen, P., Mikkilä,J., Vanhanen, J., Aalto, J., Hakola, H., Makkonen, U., Ruuskanen, T., Mauldin, R. L., Duplissy, J.,
050   Vehkamäki, H., Bäck, J., Kortelainen, A., Riipinen, I., Kurten, T., Johnston, M. V., Smith, J. N., Ehn, M., Mentel, T. F., Lehtinen, K. E. J., Laaksonen, A., Kerminen, V.-M., and Worsnop, D. R.: Direct Observations of Atmospheric Aerosol Nucleation, Science, 339, 943–946, https://doi.org/10.1126/science.1227385, 2013.

Kürten, A., Rondo, L., Ehrhart, S., and Curtius, J.: Calibration of a chemical ionization mass spectrometer for the
055   measurement of gaseous sulfuric acid, J. Phys. Chem. A, 116, 6375–6386, doi:10.1021/jp212123n, 2012.

Kürten, A., Jokinen, T., Simon, M., Sipilä, M., Sarnela, N., Junninen, H., Adamov, A., Almeida, J., Amorim, A., Bianchi, F., Breitenlechner, M., Dommen, J., Donahue, N. M., Duplissy, J., Ehrhart, S., Flagan, R. C., Franchin, A., Hakala, J., Hansel, A., Heinritzi, M., Hutterli, M., Kangasluoma, J., Kirkby, J., Laaksonen, A., Lehtipalo, K., Leiminger, M., Makhmutov, V.,

19

060   Mathot, S., Onnela, A., Petäjä, T., Praplan, A. P., Riccobono, F., Rissanen, M. P., Rondo, L., Schobesberger, S., Seinfeld, J. H., Steiner, G., Tomé, A., Tröstl, J., Winkler, P. M., Williamson, C., Wimmer, D., Ye, P., Baltensperger, U., Carslaw, K. S., Kulmala, M., Worsnop, D. R., and Curtius, J.: Neutral molecular cluster formation of sulfuric acid-dimethylamine observed in real-time under atmospheric conditions, P. Natl. Acad. Sci. USA, 111, 15019–15024, https://doi.org/10.1073/pnas.1404853111, 2014.

065

Kyrö, E.-M. Väänänen, R., Kerminen, V.-M., Virkkula, A., Petäjä, T., Asmi, A., Dal Maso, M., Nieminen, T., Juhola, S., Shcherbinin, A., Riipinen, I., Lehtipalo, K., Keronen, P., Aalto, P. P., Hari, P., and Kulmala, M.: Trends in new particle forma-tion in eastern Lapland, Finland: effect of decreasing sulfur emis-sions from Kola Peninsula. Atmos. Chem. Phys., 14, 4383–4396, https://doi.org/10.5194/acp-14-4383-2014, 2014.

070

Lehtipalo, K., Leppä, J., Kontkanen, J., Kangasluoma, J., Franchin, A., Wimmer, D., Schobesberger, S., Junninen, H., Petäjä, T., Sipilä, M., Mikkilä, J., Vanhanen, J., Worsnop, D. R., and Kulmala, M.: Methods for determining particle size distribution and growth rates between 1 and 3 nm using the Particle Size Magnifier, Boreal Environ. Res., 19, 215–236, 2014.

075

Mauldin III, R. L., Berndt, T., Sipilä, M., Paasonen, P., Petäjä, T., Kim, S., Kurtén, T., Stratmann, F., Kerminen, V.-M., and Kulmala, M.: A new atmospherically relevant oxidant, Nature, 488, 193–196, doi:10.1038/nature11278, 2012.

Merikanto, J., Spracklen, D. V., Mann, G. W., Pickering, S. J., and Carslaw, K. S.: Impact of nucleation on global CCN,
080   Atmos. Chem. Phys., 9, 8601–8616, doi:10.5194/acp-9-8601-2009, 2009.

Mirme, S. and Mirme, A.: The mathematical principles and design of the NAIS – a spectrometer for the measurement of cluster ion and nanometer aerosol size distributions, Atmos. Meas. Tech., 6, 1061–1071, doi:10.5194/amt-6-1061-2013, 2013.

085

Paatero, J., Dauvalter, V., Derome, J., Lehto, J., Pasanen, J., Vesala, T., Miettinen, J., Makkonen, U., Kyrö, E.-M., Jernström, J., Isaeva, L., and Derome, K.: Effects of Kola air pollution on the environment in the western part of the Kola peninsula and Finnish Laplad: final report, Finnish Meteorological Institute Reports, 6, 1–26, 2008.

090   Rose, C., Zha, Q., Dada, L., Yan, C., Lehtipalo, K., Junninen, H., Mazon, S. B., Jokinen, T., Sarnela, N., Sipilä, M., Petäjä, T., Kerminen, V.-M., Bianchi, F., and Kulmala, M.: Observations of biogenic ion-induced cluster formation in the atmosphere, Sci. Adv., 4, 5218, https://doi.org/10.1126/sciadv.aar5218, 2018.

Schobesberger, S., Franchin, A., Bianchi, F., Rondo, L., Duplissy, J., Kürten, A., Ortega, I. K., Metzger, A., Schnitzhofer,
095 R., Almeida, J., Amorim, A., Dommen, J., Dunne, E. M., Ehn, M., Gagné, S., Ickes, L., Junninen, H., Hansel, A., Kerminen,
V.-M., Kirkby, J., Kupc, A., Laaksonen, A., Lehtipalo, K., Mathot, S., Onnela, A., Petäjä, T., Riccobono, F., Santos, F. D.,
Sipilä, M., Tomé, A., Tsagkogeorgas, G., Viisanen, Y., Wagner, P. E., Wimmer, D., Curtius, J., Donahue, N. M.,
Baltensperger, U., Kulmala, M., and Worsnop, D. R.: On the composition of ammonia-sulfuric-acid ion clusters during
aerosol particle formation, Atmos. Chem. Phys., 15, 55–78, doi:10.5194/acp-15-55-2015, 2015.
100

Solarin, S.A., Tiwari, A.: Convergence in Sulphur Dioxide (SO$_2$) Emissions Since 1850 in OECD Countries: Evidence from
a New Panel Unit Root Test. Environ Model Assess 25, 665–675, https://doi.org/10.1007/s10666-019-09687-5, 2020.

Sipilä, M., Sarnela, N., Jokinen, T., Henschel, H., Junninen, H., Kontkanen, J., Richters, S., Kangasluoma, J., Franchin, A.,
105 Peräkylä, O., Rissanen, M. P., Ehn, M., Vehkamäki, H., Kurten, T., Berndt, T., Petäjä, T., Worsnop, D., Ceburnis, D.,
Kerminen, V.-M., Kulmala, M., and O'Dowd, C.: Molecular-scale evidence of aerosol particle formation via sequential
addition of HIO3, Nature, 537, 532–534, https://doi.org/10.1038/nature19314, 2016.

Stein, A. F., R. R. Draxler, G. D. Rolph, B. J. B. Stunder, M. D. Cohen, and F. Ngan, 2015: NOAA's HYSPLIT
110 Atmospheric Transport and Dispersion Modeling System. Bull. Amer. Meteor. Soc., 96, 2059–2077,
https://doi.org/10.1175/BAMS-D-14-00110.1.

Tammet, H., Hõrrak, U., Laakso, L., and Kulmala, M.: Factors of air ion balance in a coniferous forest according to
measure-ments in Hyytiälä, Finland, Atmos. Chem. Phys., 6, 3377–3390, doi:10.5194/acp-6-3377-2006, 2006.
115

Tuovinen J.-P., Laurila, T., and Lättilä H.: Impact of the sulphur dioxide sources in the Kola peninsula on air quality in
northernmost Europe, Atmospheric Environment, 27A, No. 9, 1379-1395, 1993.

Vehkamäki, H., McGrath, M. J., Kurtén, T., Julin, J., Lehtinen K.E.J., and Kulmala, M.: Rethinking the application of the
120 first nucleation theorem to particle formation. J. Chem. Phys. 136, 094107, https://doi.org/10.1063/1.3689227, 2012.

Wang , M , Kong , W , Marten , R , He , X-C , Chen , D , Pfeifer , J , Heitto , A , Kontkanen , J , Dada , L , Kuerten , A , Yli-
Juuti , T , Manninen , H E , Amanatidis , S , Amorim , A , Baalbaki , R , Baccarini , A , Bell , D M , Bertozzi , B ,
Braekling , S , Brilke , S , Murillo , L C , Chiu , R , Chu , B , De Menezes , L-P , Duplissy , J , Finkenzeller , H , Carracedo ,
125 L G , Granzin , M , Guida , R , Hansel , A , Hofbauer , V , Krechmer , J , Lehtipalo , K , Lamkaddam , H , Lampimaki , M ,
Lee , C P , Makhmutov , V , Marie , G , Mathot , S , Mauldin , R L , Mentler , B , Mueller , T , Onnela , A , Partoll , E ,
Petaja , T , Philippov , M , Pospisilova , V , Ranjithkumar , A , Rissanen , M , Rorup , B , Scholz , W , Shen , J , Simon , M ,

21

Sipila , M , Steiner , G , Stolzenburg , D , Tham , Y J , Tome , A , Wagner , A C , Wang , D S , Wang , Y , Weber , S K , Winkler , P M , Wlasits , P J , Wu , Y , Xiao , M , Ye , Q , Zauner-Wieczorek , M , Zhou , X , Volkamer , R , Riipinen , I ,
130 Dommen , J , Curtius , J , Baltensperger , U , Kulmala , M , Worsnop , D R , Kirkby , J , Seinfeld , J H , El-Haddad , I , Flagan , R C & Donahue , N M: Rapid growth of new atmospheric particles by nitric acid and ammonia condensation, Nature , 581 , 184-189, https://doi.org/10.1038/s41586-020-2270-4, 2020.

Weber, R. J., McMurry, P. H., Eisele, F. L., and Tanner, D. J.: Measurement of expected nucleation precursor species and 3-
135 500-nm diameter particles at Mauna Loa observatory, Hawaii, J. Atmos. Sci., 52, 2242–2257, 1995.

Wiedensohler, A., Birmili, W., Nowak, A., Sonntag, A., Weinhold, K., Merkel, M., Wehner, B., Tuch, T., Pfeifer, S., Fiebig, M., Fjäraa, A. M. Asmi, E., Sellegri, K., Depuy, R., Venzac, H., Vil lani, P., Laj, P., Aalto, P., Ogren, J. A. Swietlicki, E., Williams, P., Roldin, P., Quincey, P., Hüglin, C., Fierz-Schmidhauser, R., Gysel, M., Weingartner, E., Riccobono, F.,
140 Santos, S., Grüning, C., Faloon, K., Beddows, D., Harrison, R., Monahan, C., Jennings, S. G., O'Dowd, C. D., Marinoni, A., Horn, H.-G., Keck, L., Jiang, J., Scheckman, J., McMurry, P. H., Deng, Z., Zhao, C. S., Moerman, M., Henzing, B., de Leeuw, G., Löschau, G., and Bastian, S.: Mobility particle size spectrometers: harmonization of technical standards and data structure to facilitate high quality long-term observations of atmospheric particle number size distributions, Atmos. Meas. Tech., 5, 657–685, doi:10.5194/amt- 5-657-2012, 2012.
145
Yan, C., Dada, L., Rose, C., Jokinen, T., Nie, W., Schobesberger,S., Junninen, H., Lehtipalo, K., Sarnela, N., Makkonen, U., Gar-mash, O., Wang, Y., Zha, Q., Paasonen, P., Bianchi, F., Sipilä, M.,Ehn, M., Petäjä, T., Kerminen, V.-M., Worsnop, D. R., and Kulmala, M.: The role of H_2SO_4-NH_3 anion clusters in ion-inducedaerosol nucleation mechanisms in the boreal forest, Atmos.Chem. Phys., 18, 13231–13243, https://doi.org/10.5194/acp-18-13231-2018, 2018.
150
Yao, L., Garmash, O., Bianchi, F., Zheng, J., Yan, C., Kontkanen, J., Junninen, H., Mazon, S. B., Ehn, M., Paasonen, P., Sipilä, M., Wang, M., Wang, X., Xiao, S., Chen, H., Lu, Y., Zhang, B., Wang, D., Fu, Q., Geng, F., Li, L., Wang, H., Qiao, L., Yang, X., Chen, J., Kerminen, V.-M., Petäjä, T., Worsnop, D. R., Kulmala, M., and Wang, L.: Atmospheric new particle formation from sulfuric acid and amines in a Chinese megacity, Science, 361, 278–281,
155 https://doi.org/10.1126/science.aao4839, 2018.

160

A = Värriö
B = Nikel
C = Zapolyarny
D = Kovdor
E = Monchegorsk
F = Olenogorsk
G = Apatity
H = Kandalaksha
I = Kirovsk

Figure 1. Map of the study area. Industrial cities of Nikel, Zapoljarnij, Monchegorsk, Kandalaksha have large-scale metal smelters emitting vast quantities of SO$_2$ into the atmosphere. Kovdor and Olenegorsk mines produce nickel/iron ore, but have no smelter industry. Kirovsk and Apatity are phosphate mining and processing sites.
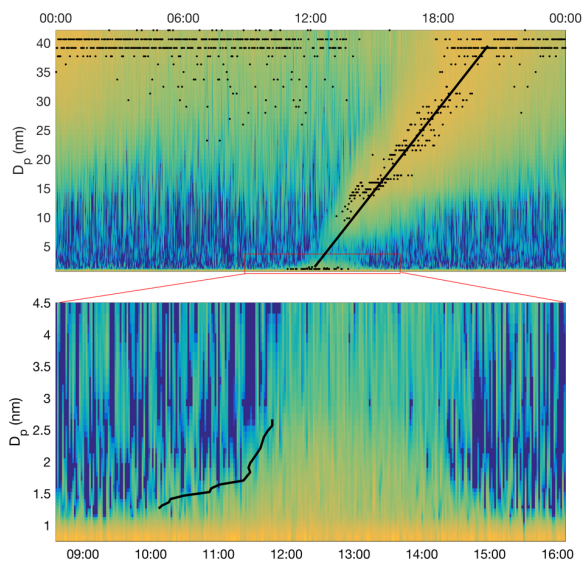
Figure 2. Particle formation event recorded by NAIS (negative ions) on 29. January 2020 depicted on linear diameter scale. Average growth rate determination by linear fitting to growing nucleation mode yields the average growth rate of 5 nm h^{-1} (upper panel) while 50-% appearance time method (Lehtipalo et al., 2014) applied in cluster mode growth yields growth rates from ca. 0.35 to 1.8 nm h^{-1} (lower panel). Both methods likely overestimate true growth rate since particle size distribution is affected by air mass advection. Therefore, the growth rate applied in nucleation rate calculations is derived from sulphuric acid concentration (Stolzenburg et al., 2020).
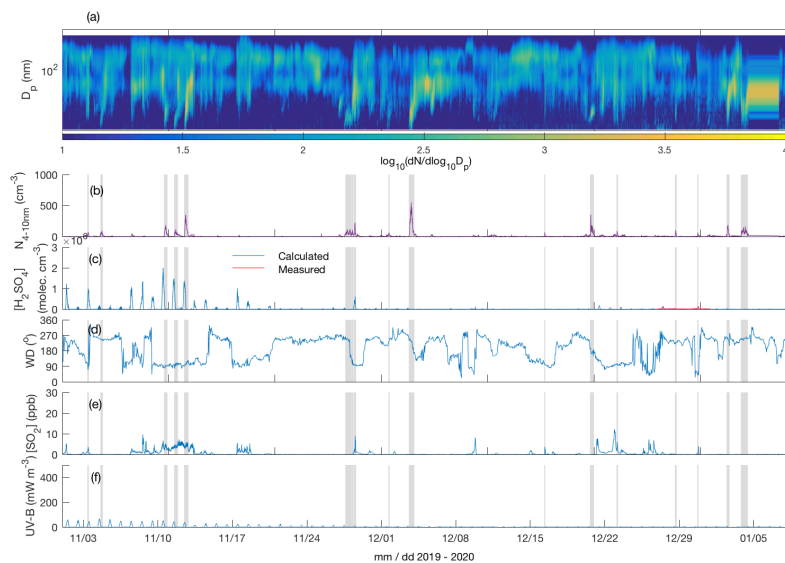
Figure 3. Aerosol size distribution (4-700 nm) (a), small particle (4-10 nm) concentration (b), measured (only 27.12.-31.12.2019) and calculated (Dada et al., 2020) sulphuric acid concentration (c), wind direction (d), [SO₂] (e) and UV-B radiation (f) between 1.11.2019 – 07.1.2020. Gray shaded areas depict the times with observed < 10 nm new particle formation. The polar night (sun constantly below horizon) period is from 9.12.2019 to 4.1.2020.
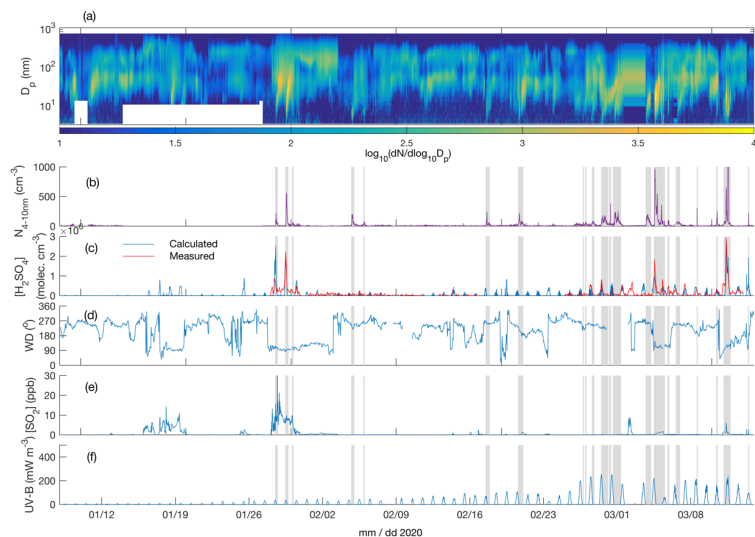
190 **Figure 4. A**erosol size distribution (4-700 nm) (a), small particle (4-10 nm) concentration (b), measured and calculated (Dada et al., 2020) sulphuric acid concentration (c), wind direction (d), [SO₂] (e) and UV-B radiation (f) between 8.1.2020 – 15.3.2020. Gray shaded areas depict the times with observed < 10 nm new particle formation.
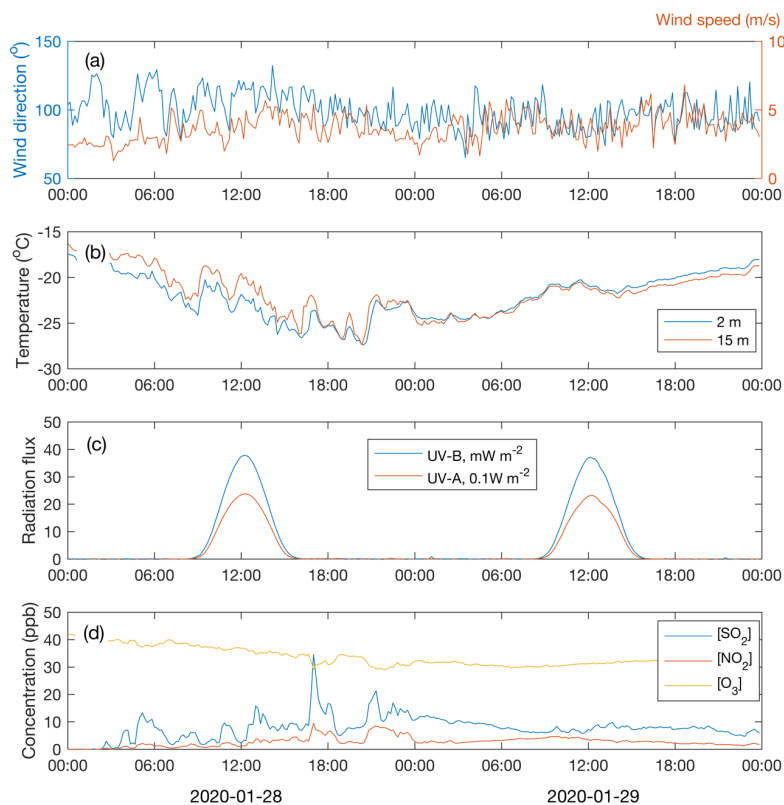
205 Figure 5. Wind speed and direction at the 16-m height (a), air temperature at two heights (b), UV-B and UVA radiation (c) and concentrations of SO_2, NO_2, O_3 (d) during the examination period.

Arrival height 50 m AGL

Arrival height 250 m AGL

Legend:
- ○ Värriö
- ■ Nikel
- ■ Montchegorsk
- ■ Kantalahti
- ■ Koutero
- – – 30.1. 00UTC
- —— 29.1. 18 UTC
- —— 29.1. 12 UTC
- ⋯⋯ 29.1. 06 UTC
- – – 29.1. 00 UTC
- —— 28.1. 18 UTC
- —— 28.1. 12 UTC
- ⋯⋯ 28.1. 06 UTC
- – – 28.1. 00 UTC
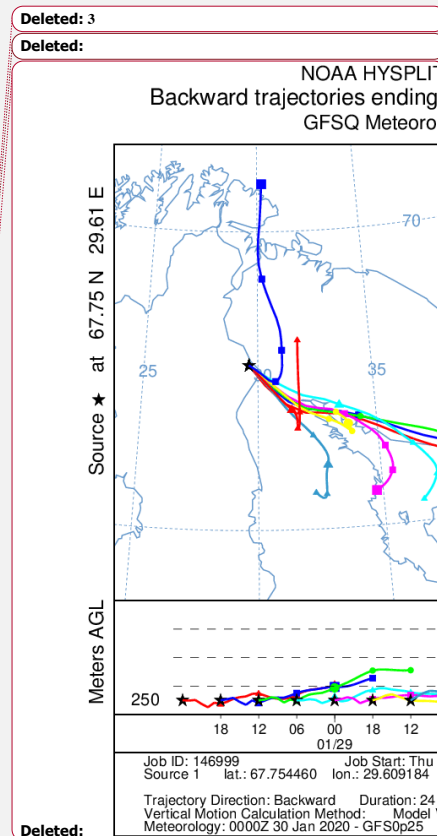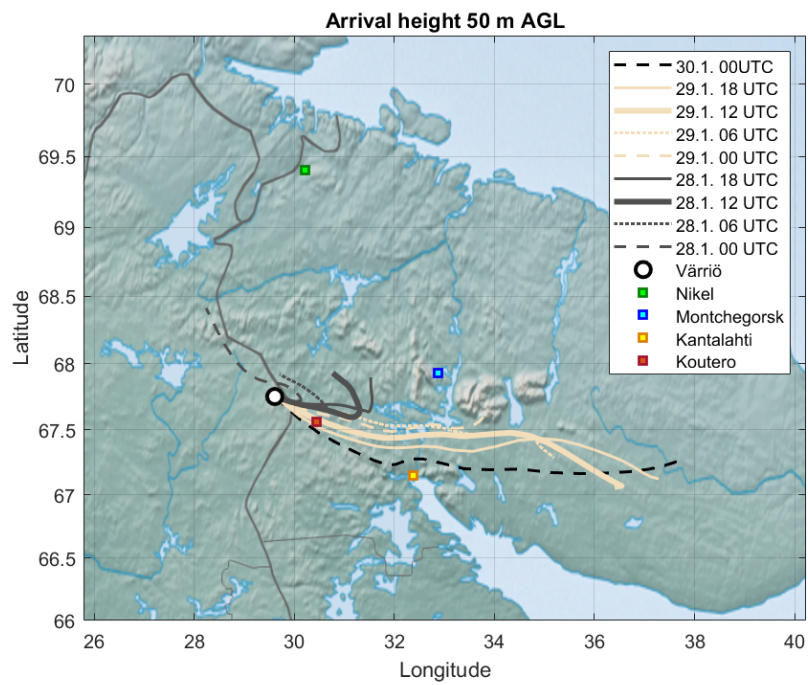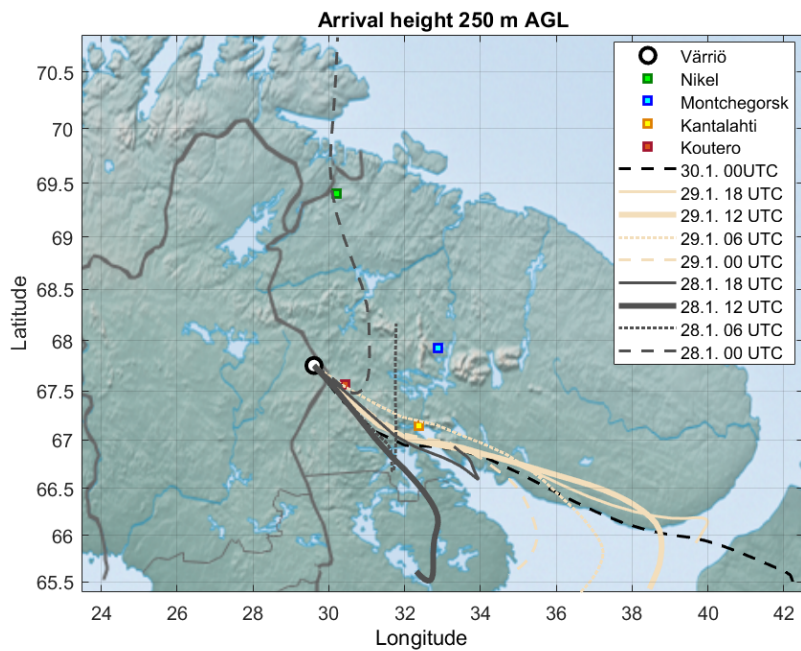
Figure 6. 24-hour back trajectories with an arrival height of 50 m (a) and 250 m (b) above ground level (AGL) and with an arrival time between 28th January 00:00 and 30th January 00:00.

| Deleted: 4 |
| Deleted: ing |

29
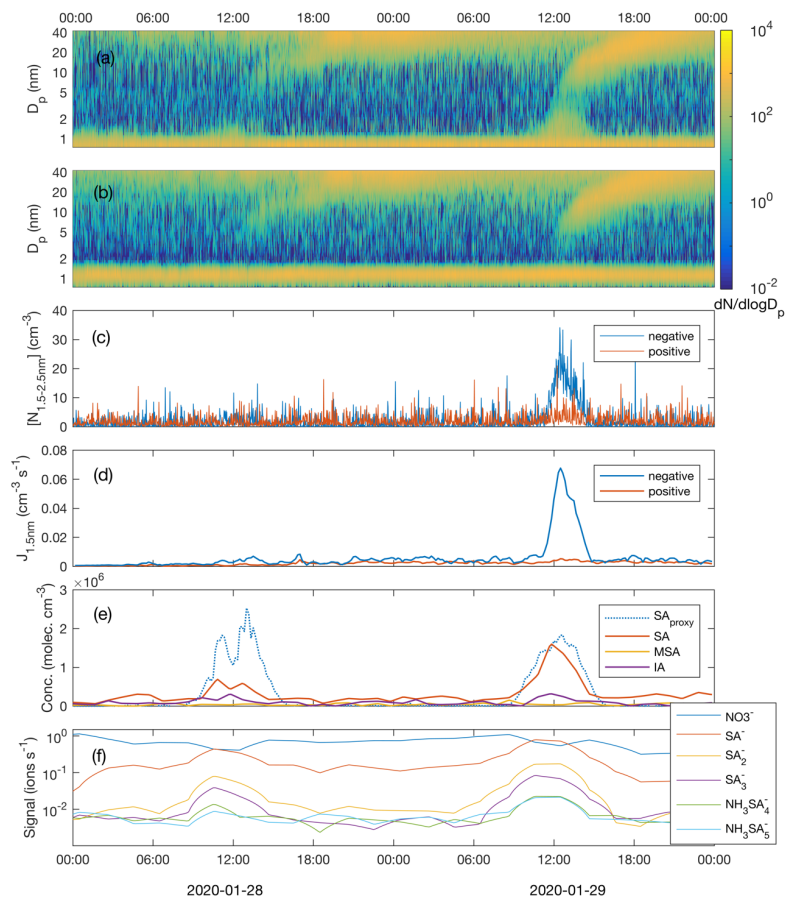
Figure 7. Size distribution of negative (a) and positive (b) clusters and particles, concentration of freshly nucleated, charged 1.5-2.5 nm clusters (c), formation rate of negative and positive 1.5 nm clusters (d), measured concentrations of sulphuric acid (H_2SO_4), methane sulphonic acid (MSA) and iodic acid (HIO_3) as well as sulphuric acid concentration estimated by proxy calculation (e), and the signal intensity of nucleating ion clusters with different composition (f) during the examination period.

225

230
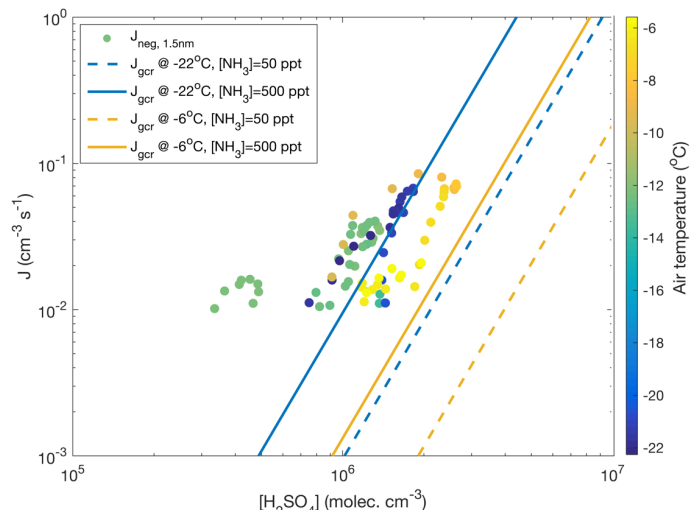
Figure 8. 1-hour average negative ion-induced nucleation rates calculated vs. calculated sulphuric acid concentration (Dada et al., 2020) for days with visible and clear nucleation events (11.-12.11.2019, 18.-19.11.2019, 28.-29.1.2020, 13.3.2020) colored according to air temperature. Nucleation rate of 10^{-2} cm^{-3}s^{-1} was used as a threshold for reliable determination below which instrument noise becomes predominant. No positive ion-induced nucleation was observed. For comparison, total (negative, positive and neutral) nucleation rates J_{gcr} calculated based on CLOUD parameterization (Dunne et al., 2016) are presented. Calculation assumes a ground-level galactic cosmic ray ionization rate of 1.8 ion pairs cm^{-3} s^{-3} and no contribution from terrestrial radioactivity. Calculation was performed at -22°C and at -6°C assuming 50 or 500 ppt ammonia concentration. Despite the fact that in these conditions the total J_{gcr} is approximately equal to negative ion-induced J_{neg}, our J values slightly exceed those that would be expected based on parameterization assuming ammonia concentration does not exceed 500 ppt. However, the disagreement is such small for atmospheric nucleation rate measurement (which does not account for e.g. airmass mixing and transportation) that it should not be considered to conflict with the proposed mechanism.
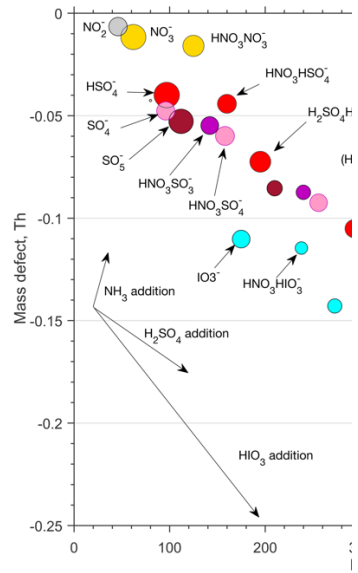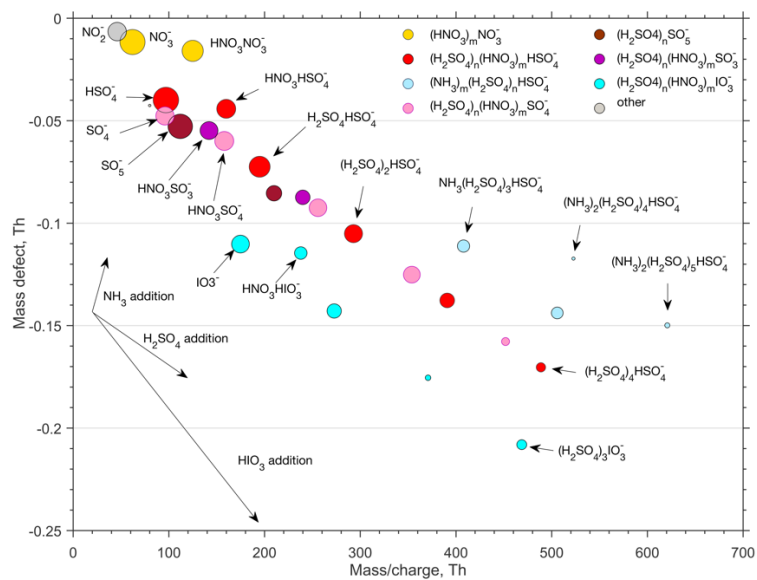

Deleted:
Figure 6. Mass defect plot (with 2 h effective integration time) of ann anion cluster distribution recorded by the APi-TOF during intensive cluster formation on 29th of January 2020. See text for detailed description.

31

Figure 9. Mass defect plot (with 2 h effective integration time) of an anion cluster distribution recorded by the APi-TOF during intensive cluster formation on 29th of January 2020. See text for detailed description.
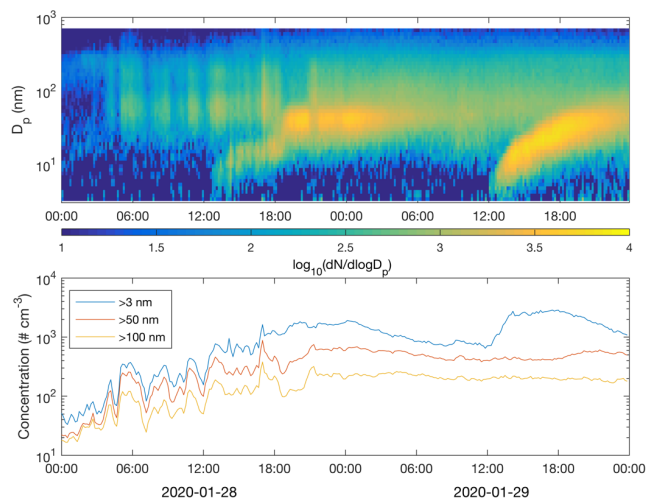
Formatted: English (US)

32

Figure 10. Particle number size distribution (a) and concentrations of particles larger than 3 nm, 50 nm and 100 nm (b) recorded by the DMPS.
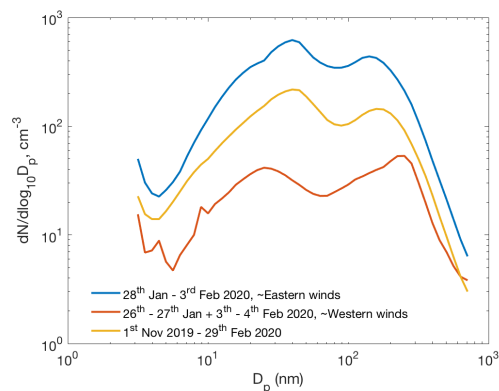
Figure 11. Average particle number size distributions during the ~one-week period of easterly winds (28th Jan – 3rd Feb 2020), during the preceding and succeeding time period with westerly winds, and average number size distribution between 1st November

Deleted: 7

Deleted: 8

Deleted: the ca. 1

Deleted: n

Deleted: n

and 29th February. New particle formation in the eastern air mass significantly increases the concentrations of particles in every size class.

270

Page 7: [1] Deleted	Microsoft Office User	6/15/21 3:17:00 PM

Page 7: [1] Deleted	Microsoft Office User	6/15/21 3:17:00 PM

Page 7: [1] Deleted	Microsoft Office User	6/15/21 3:17:00 PM

Page 7: [1] Deleted	Microsoft Office User	6/15/21 3:17:00 PM

Page 7: [2] Deleted	Kerminen, Veli-Matti	5/24/21 4:03:00 PM

Page 7: [2] Deleted	Kerminen, Veli-Matti	5/24/21 4:03:00 PM

Page 7: [3] Deleted	Kerminen, Veli-Matti	5/24/21 4:04:00 PM

Page 7: [3] Deleted	Kerminen, Veli-Matti	5/24/21 4:04:00 PM

Page 7: [3] Deleted	Kerminen, Veli-Matti	5/24/21 4:04:00 PM

Page 7: [3] Deleted	Kerminen, Veli-Matti	5/24/21 4:04:00 PM

Page 7: [4] Deleted	Kerminen, Veli-Matti	5/24/21 4:06:00 PM

Page 7: [4] Deleted	Kerminen, Veli-Matti	5/24/21 4:06:00 PM

Page 7: [4] Deleted	Kerminen, Veli-Matti	5/24/21 4:06:00 PM

Page 7: [5] Formatted	Microsoft Office User	6/15/21 1:10:00 PM

Font color: Text 1

Page 7: [5] Formatted	Microsoft Office User	6/15/21 1:10:00 PM

Font color: Text 1

Page 7: [5] Formatted	Microsoft Office User	6/15/21 1:10:00 PM

Font color: Text 1

Page 7: [6] Deleted	Microsoft Office User	6/15/21 1:09:00 PM

Page 7: [6] Deleted	Microsoft Office User	6/15/21 1:09:00 PM

Page 7: [7] Deleted	Kerminen, Veli-Matti	5/24/21 4:09:00 PM

Page 7: [7] Deleted	Kerminen, Veli-Matti	5/24/21 4:09:00 PM

Page 7: [7] Deleted	Kerminen, Veli-Matti	5/24/21 4:09:00 PM

Page 7: [8] Deleted	Microsoft Office User	6/15/21 3:22:00 PM

Page 7: [8] Deleted	Microsoft Office User	6/15/21 3:22:00 PM

Page 7: [9] Deleted	Kerminen, Veli-Matti	5/24/21 4:41:00 PM

Page 7: [9] Deleted	Kerminen, Veli-Matti	5/24/21 4:41:00 PM

Page 7: [9] Deleted	Kerminen, Veli-Matti	5/24/21 4:41:00 PM

Page 7: [9] Deleted	Kerminen, Veli-Matti	5/24/21 4:41:00 PM

Page 7: [9] Deleted	Kerminen, Veli-Matti	5/24/21 4:41:00 PM

Page 7: [9] Deleted	Kerminen, Veli-Matti	5/24/21 4:41:00 PM

Page 7: [9] Deleted	Kerminen, Veli-Matti	5/24/21 4:41:00 PM

Page 7: [9] Deleted	Kerminen, Veli-Matti	5/24/21 4:41:00 PM

Page 7: [9] Deleted	Kerminen, Veli-Matti	5/24/21 4:41:00 PM

Page 7: [9] Deleted	Kerminen, Veli-Matti	5/24/21 4:41:00 PM

Page 7: [10] Deleted	Microsoft Office User	6/15/21 3:23:00 PM

Page 7: [10] Deleted	Microsoft Office User	6/15/21 3:23:00 PM

Page 7: [11] Deleted	Kerminen, Veli-Matti	5/24/21 4:50:00 PM

Page 7: [11] Deleted	Kerminen, Veli-Matti	5/24/21 4:50:00 PM

Page 7: [11] Deleted	Kerminen, Veli-Matti	5/24/21 4:50:00 PM

Page 7: [11] Deleted	Kerminen, Veli-Matti	5/24/21 4:50:00 PM

Page 7: [12] Deleted	Kerminen, Veli-Matti	5/24/21 4:53:00 PM

Page 7: [12] Deleted	Kerminen, Veli-Matti	5/24/21 4:53:00 PM